

# Missing sea-level rise in southeast Greenland during and since the Little Ice Age

Sarah A. Woodroffe<sup>1</sup>, Leanne M. Wake<sup>2</sup>, Kristian K. Kjeldsen<sup>3</sup>, Natasha L.M. Barlow<sup>4</sup>, Antony J. Long<sup>1</sup>, Kurt H. Kjær<sup>5</sup>

<sup>1</sup>Department of Geography, Durham University, Lower Mountjoy, South Road, Durham, DH1 3LE, UK, s.a.woodroffe@durham.ac.uk

<sup>2</sup>Department of Geography and Environmental Sciences, Northumbria University, Ellison Place, Newcastle upon Tyne, NE1 8ST, UK, leanne.wake@northumbria.ac.uk

<sup>3</sup>Geological Survey of Denmark and Greenland (GEUS), 1350 Copenhagen K, Denmark, kkk@geus.dk

<sup>4</sup>School of Earth and Environment, University of Leeds, LS2 9JT, UK, n.l.m.barlow@leeds.ac.uk

<sup>5</sup>GeoGenetics, Globe Institute, University of Copenhagen, 1350 Copenhagen K, Denmark, kurtk@sund.ku.dk

*Correspondence to:* Sarah A. Woodroffe (s.a.woodroffe@durham.ac.uk)

## Abstract

The Greenland Ice Sheet has been losing mass at an accelerating rate over the past two decades. Understanding ice mass and glacier changes during the preceding several hundred years, prior to geodetic measurements, is more difficult because evidence of past ice extent in many places was later overridden. Saltmarshes provide the only continuous records of Relative Sea Level (RSL) from close to the Greenland Ice Sheet that span the period of time during and since the Little Ice Age (LIA) and can be used to reconstruct ice mass gain and loss over recent centuries. Saltmarsh sediments collected at the mouth of Dronning Marie Dal, close to the Greenland Ice Sheet margin in southeast Greenland, record RSL changes over the past c. 300 years through changing sediment and diatom stratigraphy. These RSL changes record a combination of processes that are dominated by local/regional changes in

Greenland Ice Sheet mass balance during this critical period that spans the maximum of the LIA and 20th Century warming. In the early part of the record (1725-1762 CE) the rate of RSL rise is higher than reconstructed from the closest isolation basin at Timmiarmiut, but between 1762-1880 CE the RSL rate is within the error range of rate of RSL change recorded in the isolation basin. RSL begins to slowly fall around 1880 CE, with a total amount of RSL fall of  $0.09 \pm 0.1$  m in the last 140 years. Modelled RSL, which takes into account contributions from post-LIA Greenland Ice Sheet Glacio-isostatic Adjustment (GIA), ongoing deglacial GIA, the global non-ice sheet glacial melt fingerprint, contributions from thermosteric effects, the Antarctic mass loss sea-level fingerprint and terrestrial water storage, over-predicts the amount of RSL fall since the end of the LIA by at least 0.5 m. The GIA signal caused by post-LIA Greenland Ice Sheet mass loss is by far the largest contributor to this modelled RSL, and error in its calculation has a large impact on RSL predictions at Dronning Marie Dal. We cannot reconcile the modelled RSL and the saltmarsh observations, even when moving the termination of the LIA to 1700 CE and reducing the post-LIA Greenland mass loss signal by 30 %, and a ‘budget residual’ of  $\sim 3$  mm/yr since the end of the LIA remains unexplained. This new RSL record backs up other studies which suggest that there are significant regional differences in the timing and magnitude of the response of the Greenland Ice Sheet to the climate shift from the LIA into the 20<sup>th</sup> Century.

Keywords: Greenland, relative sea level, saltmarsh, glacio-isostatic adjustment, Little Ice Age, sea-level budget

## **1. Introduction**

Studies using a range of different geodetic methods all agree that the Greenland Ice Sheet (GrIS) has been losing mass at an accelerating rate over the past two decades (Bevis et al., 2019, 2012; Chen et al., 2021; Khan et al., 2015; Moon et al., 2012; Pritchard et al., 2009; The IMBIE Team, 2020; van den Broeke et al., 2009). There is however less known about when and at what rate ice mass loss occurred in Greenland during the last millennium until the start of the satellite and GPS eras, when Greenland underwent periods of climate warming and cooling (Briner et al., 2020; Khan et al., 2020; Kjær et al., 2022). Using Little Ice Age (LIA) trimlines and stereo-photogrammetric imagery recorded between

1978-1987, Kjeldsen et al. (2015) estimated an average Greenland-wide total ice mass loss of c. 75 Gt/yr during the 20th Century. However, understanding how the rate of mass loss varied during the 20<sup>th</sup> Century is more complex because it requires us to put a date on the end of the LIA, and to find a way of reconstructing mass loss fluctuations without the help of continuous geodetic data. Understanding ice mass and glacier changes during the preceding several hundred years is even more difficult because evidence of past ice sheet extent in many places has been overridden by later advances (Briner et al., 2011; Kjær et al., 2022).

Salt marshes in nearfield settings record the timing and magnitude of fluctuations in ice mass during the last few centuries through changes in relative sea-level (RSL) (e.g. Long et al., 2012). RSL reflects the interplay of different cryosphere and oceanic processes but the dominant process close to an ice sheet is the visco-elastic signature of local and regional mass changes through time (Farrell and Clark, 1976). Salt marshes form in the upper part of the intertidal zone and can continuously accumulate organic sediment (Allen, 2000). Salt marshes in Greenland are generally small features with a very short growing season, low sedimentation rates and may be affected by interactions with winter shore-fast ice (Lepping and Daniëls, 2007). However, they can survive in these conditions and provide the only continuous records of RSL from close to the GrIS that span the period during and since the LIA and can be used to reconstruct ice mass gain and loss over recent centuries (Long et al., 2012, 2010; Woodroffe and Long, 2009).

This study reports for the first time a continuous RSL record over the past ~300 years from a salt marsh within 5 km of the ice sheet margin in southeast Greenland. The sediments and plant remains in the marsh record RSL fluctuations over the last few hundred years and therefore provide a unique record of changes in regional RSL during and since the LIA in Greenland. We predict local RSL changes by creating a sea-level budget which includes predictions from a Glacio-Isostatic Adjustment (GIA) model with c. 430 Gt ice mass loss in southeast Greenland between the end of the LIA and 2010 (as defined by Kjeldsen et al., 2015), and estimates of other contributions since the end of the LIA including mass loss from Greenland peripheral glaciers, non-Greenland ice, the thermosteric contribution and the effect of terrestrial water storage in the 20<sup>th</sup> and 21<sup>st</sup> Centuries. Comparing the modelled sea-level budget and

the saltmarsh data provides an opportunity to consider potential errors in both methods and suggest how we might bring model and data estimates closer together, as well as develop better understanding of the nature of historical RSL in southeast Greenland and implications for coastline response to future, enhanced GrIS and peripheral glacier melt.

## 2. Study site and methods

### 2.1 Field site and glacial history of the region

The saltmarsh record is from 63.470°N, -41.925°W at the head of Dronning Marie Dal in southeast Greenland (Figure 1A,B, Fig 2). The saltmarsh is fed by freshwater and sediment from Dronning Marie Dal, a formerly glaciated valley that drains part of the nearby Skinfaxe outlet glacier. Dronning Marie Dal is at the head of the 50 km long marine fjord Søndre Skjoldungesund which together with Nørre Skjoldungesund encompass the glaciated island of Skjoldungen (Figure 1C). The northern fjord has a bedrock sill mid-fjord at c. 215 m below sea level, while the southern fjord has a narrow central section with a sill located at 77 m below sea level (Kjeldsen et al., 2017). The narrow stretch connecting the two fjords at their inland extent is generally shallow, sheltering the salt marsh at Dronning Marie Dal. The region is dominated by long, steep-sided marine fjords with the GrIS ending at the coast in marine-terminating outlet glaciers.

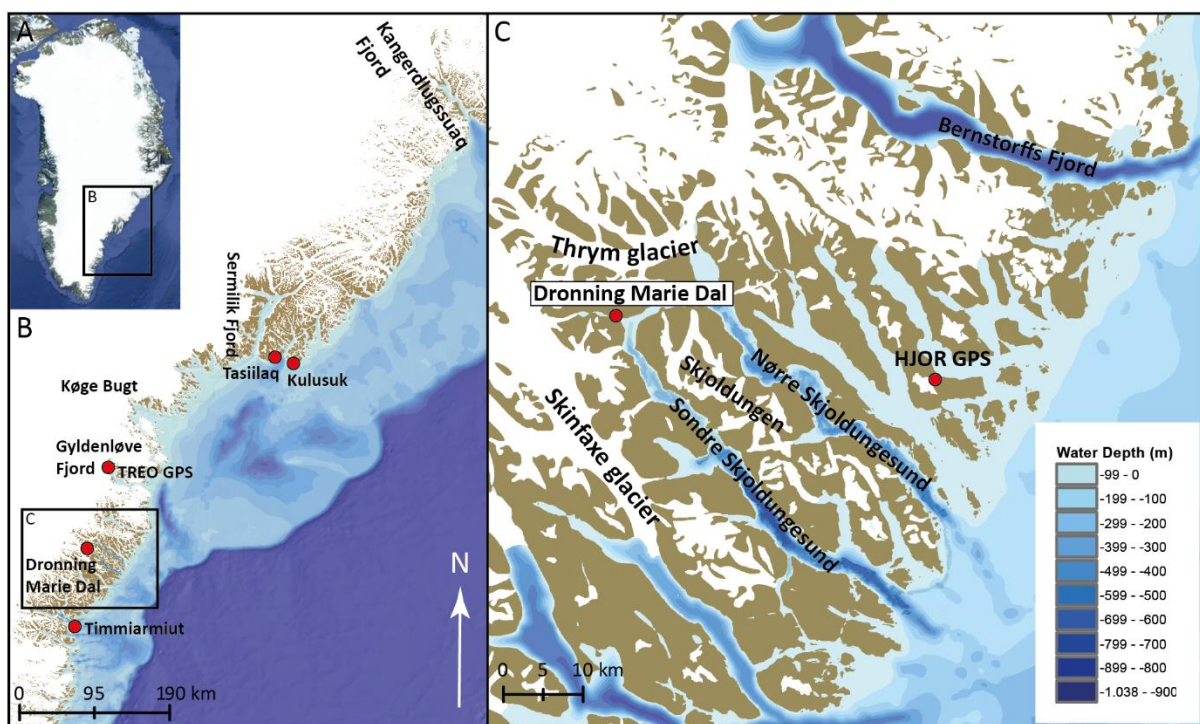


Figure 1. A) Map of Greenland © Google Earth, B) Southeast Greenland region showing the location of the field site (Dronning Marie Dal) alongside other studied fjords, C) Dronning Marie Dal saltmarsh at the head of Sondre Skjoldungesund, between the Skinfaxe and Thrum glacier margins.

Relatively little is known about the deglacial history of the southeast compared to the southwest of Greenland. Most work has been undertaken in the large fjords (e.g. Kangerdlugssuaq, Sermilik, Køge Bugt, Gyldenløve, Bernstorffs Fjord, Figure 1) to the north of the field area using  $^{10}\text{Be}$  measurements to reconstruct fjord deglaciation. During the LGM the ice sheet reached the shelf edge (50-80 km from the outer coast) in this region and in the offshore Kangerdlugssuaq Trough to the north of the study area the ice sheet started to retreat by c. 17 ka BP (Funder et al., 2011). Onshore deglaciation at the outer coast occurred earlier to the north (Kangerdlugssuaq - 11.8  $\pm$  1ka BP) compared to the south (Bernstorffs Fjord - 10.4  $\pm$  450 ka BP), driven by incursion of warm Atlantic water into the fjords from the Irminger Current, moderated by local coastal bathymetry and atmospheric warming during the early Holocene (Dyke et al., 2018, 2014; Hughes et al., 2012).  $^{10}\text{Be}$  dates on boulders from outer and inner Skjoldungesund suggest deglaciation here occurred in the early Holocene (inner fjord by 10.4  $\pm$  0.4 ka BP) (Levy et al., 2020). Following retreat from the shelf edge, the deglaciation model HUY3 simulates retreat onshore by 10 ka BP, which largely agrees with the field evidence from Skjoldungesund, with the ice sheet slightly inland of its LIA maximum position at 4 ka BP (Lecavalier et al., 2014). The deglacial marine limit is low in this region (c. 20-40 m) suggesting less deglacial mass loss compared to elsewhere in Greenland (Funder and Hansen, 1996). Observations of strandlines up to 75 m above sea level in this region, reported by Vogt (1933) are cut into bedrock and are highly unlikely to be of marine origin.

The HUY3 geophysical model predicts slight crustal subsidence at the coast today caused primarily by a local late Holocene neoglacial readvance (resulting in RSL rise of 1-1.5 mm/yr over the last 1000 years) (Lecavalier et al., 2014). However, a recent GPS-derived GIA model (GNET-GIA) offers an alternative solution with GIA uplift calculated at +2.8mm/yr and +3.1 mm/yr at nearby HJOR and TREO GPS sites (Figure 1), which would result in pre-20<sup>th</sup> Century RSL fall at Dronning Marie Dal (Khan et al., 2016). By comparing GPS data and absolute gravity observations over a 20-year period,

van Dam et al (2017) also suggest ongoing GIA uplift of  $+4.5 \pm 1.4$  mm/yr at Kulusuk (300 km to the north). These GIA estimates, based on modern observations, are corrected for elastic deformation in response to modern mass balance changes to predict ongoing deglacial GIA. The most recent examination of Greenland GIA model outputs and GPS data by Adhikari et al. (2021) suggests that residual uplift caused by mass loss since the Medieval Warm Period, and in particular since the LIA, accompanied by a reduced mantle viscosity on sub-centennial timescales, can explain the observed discrepancy between uplift rates from HUY3 and elastic-corrected GPS uplift rates around Greenland.

LIA moraines are situated ahead of the current frontal margins of the GrIS and local glaciers in this region and demonstrate clearly that glacial retreat has occurred during the 20th Century (Bjork et al., 2012). The instrumental temperature record from Tasiilaq indicates  $2^{\circ}\text{C}$  per decade of warming between 1919 and 1932 CE (the early twentieth-century warming (ECW)), followed by cooling during the 1950's to 1970's and steady temperature rise of  $1.3^{\circ}\text{C}$  per decade since 1993 (Bjork et al., 2012; Chylek et al., 2006; Wood and Overland, 2010). Despite these decadal temperature fluctuations, and the overall pattern of post-LIA retreat of southeast Greenland glaciers, the nearest glaciers to the field site (Skinfaxe and Thrym, Figure 1C) have been relatively stable at their present positions since at least the 1930s (Bjork et al., 2012). It is important to note however that Skinfaxe sits on a ledge in its fjord system so would require significant thinning to dislodge it from its current position and Thrym Glacier appears to be resting on a shallow bedrock rise (Bjork et al., 2012; Morlighem et al., 2017). The total ice mass loss from the two drainage basins closest to the field site (Central East and South-East in Kjeldsen et al., 2015) is 249 Gt between the end of the LIA and 1983, 134 Gt between 1983 and 2003 and 45 Gt between 2003 and 2010, based on the volume of loss from LIA trimlines and more recent air photos. There is a significant increase ( $\sim 70\%$ ) in the amount of regional mass loss during the post-1983 period compared to earlier in the 20<sup>th</sup> Century. We hypothesise that regional ice mass loss since the end of the LIA should produce a visco-elastic GIA response recorded as variable 20th century RSL change by local salt marsh sediments, such as those at Dronning Marie Dal (Figure 2).

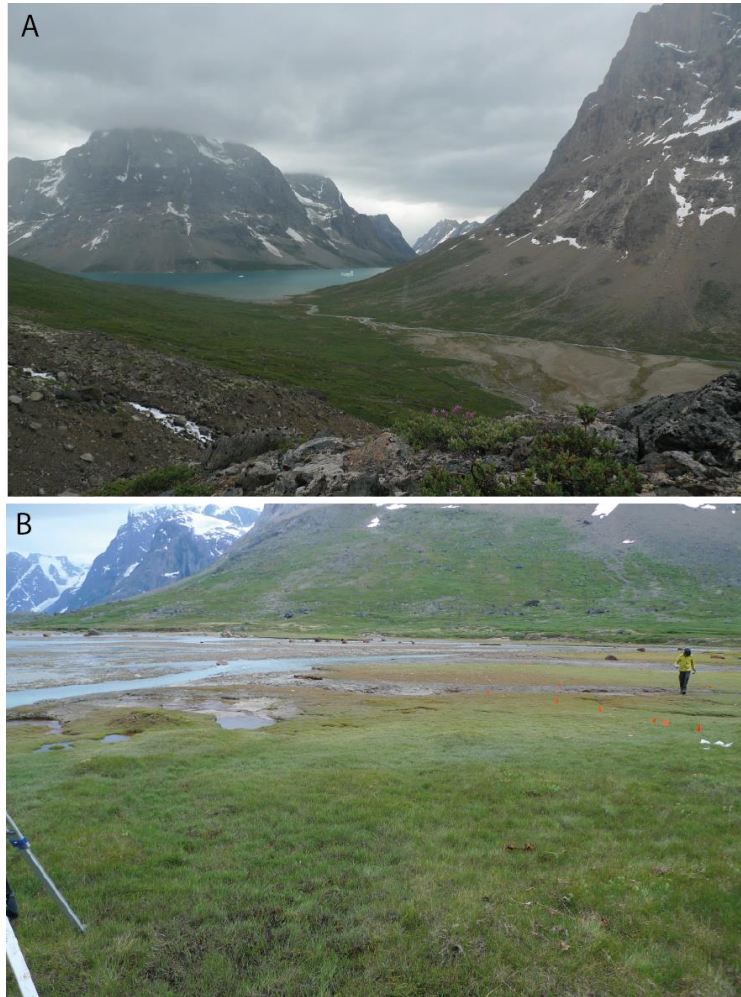


Figure 2. A) photograph looking East down the Dronning Marie Dal valley towards the head of Sondre Skoldungesund and the salt marsh where the valley meets the fjord. B) photograph of the Dronning Marie Dal salt marsh showing the low-angled relief of the marsh and zonation of salt marsh vegetation (high marsh in the foreground).

## 2.2 Reconstructing RSL using saltmarsh sediments

We collected salt marsh sediments by digging a small pit using a spade from the present-day high salt marsh at the mouth of Dronning Marie Dal (Figure 1C, 2). The analysed sediment section is 13 cm thick, with organic silt containing saltwater-tolerant diatoms situated over compacted sand-rich silt where no diatoms are present (Figure 3). We sampled the fossil sediment section at 0.25 cm intervals in the top 1 cm, and at 0.5 cm intervals further downcore to provide high-resolution RSL estimates, bearing in mind the slow rate of sedimentation in most Greenlandic salt marshes (Long et al., 2012; Woodroffe and Long, 2009). To reconstruct local RSL we investigated diatom assemblages across the

present-day salt marsh in the same location to understand changes in assemblages with elevation across the upper part of the intertidal zone (Figure 3A). We then compared these assemblages to those found through the sediment core using a visual assessment technique, that places weight on certain taxa that change abundance at clearly defined elevations (Long et al., 2012, 2010; Woodroffe and Long, 2009). The main species used to reconstruct RSL are the high marsh/freshwater species *Pinnularia intermedia*, and the high to low marsh species *Navicula cincta* and *Navicula salinarum*. Using elevation zones inhabited by key species alone to reconstruct RSL introduces artificial jumps into a RSL record when moving from a sample reconstructed from within one zone to the next sample which may be reconstructed in a different zone. To create an RSL reconstruction with no artificial jumps within it we use a smoothing function which allows the PMSE (palaeo-marsh surface elevation) to change within each zone, noting the progressive way that the key diatom taxa change up core. For instance the progressive rise in *Pinnularia intermedia* in the top 4 cm suggests smoothly falling RSL during this period. We therefore modify the PMSE results for the zoned reconstruction to allow for the progressive change seen in the diatoms (Table S2). This is backed up by the LOI data which suggests a progressive rise in organic content in the top 4 cm indicative of rising PMSE. We prefer this method over a transfer function approach (e.g. Barlow et al., 2013) because it relies on certain indicator species that occur at narrowly defined levels, but also utilises other evidence such as vertical diatom succession and the stratigraphy to interpret changes in RSL. In addition we do not tune the RSL reconstructions to present day RSL, rather the most recent index point reflects its diatom-based reconstruction and therefore present day RSL lies within the vertical error term of this reconstruction. This is done to prevent a spurious jump in recent RSL caused by a vertical offset between the mid-point in the earlier diatom-based reconstructions and the present-day marsh-surface elevation, which would happen if this was used to tune the core-top sample reconstruction.

We initially calculated the elevations of modern and fossil saltmarsh samples to mean sea level (MSL) using a high-precision dGPS. However due to technical issues with post-processing we instead rely on tidal data from Timmiarmiut (100 km to the S) and tidal predictions from Tasiilaq (300 km to the NE) collected during our fieldwork, along with knowledge about saltmarsh vegetation zonation in Greenland and their general relationship to tidal levels, to relate fossil and modern saltmarsh elevations to mean



sea level (MSL). The tidal data from Timmiarmiut show that although the timing of daily tidal fluctuations differs to predictions for Tasiilaq, the amplitude of tidal fluctuations is remarkably similar (within 0.1 m). The tidal range (lowest to highest astronomical tide) at the outer coast is approximately 3.7 m. We have some confidence therefore that tidal predictions for Tasiilaq are applicable (with a time correction) along the outer coast anywhere between Tasiilaq and Timmiarmiut, although the distances involved are large. This leaves the issue of tidal range amplification or dampening in fjord-head settings to consider, as the Dronning Marie Dal site is c. 50 km up-fjord from the open ocean (Figure 1C). This is considered elsewhere in Greenland by Richter et al., (2011) who show that this effect is variable due to fjord bathymetry and cross-section geometry, and ranges from -9 cm to +14 cm up fjord compared to the fjord mouths on the west coast in fjords of similar length to Søndre Skoldungesund. Modern saltmarsh vegetation at Dronning Marie Dal grows between 0.1 m above Highest Astronomical Tide (HAT) and 0.08 m below Mean High Water of Spring Tide (MHWST) levels, which is very similar to saltmarsh vegetation ranges we have observed elsewhere in southeast and southwest Greenland (unpublished data and Woodroffe and Long, 2010, 2009). We are therefore confident that any effect of the fjord-head setting on tidal range is small. We have not included an uncertainty estimate in our overall RSL reconstruction to reflect this, because the uncertainty in the proxy elevations is already of a similar magnitude ( $\pm 0.10$ - $0.15$  m, see Table A2 in Appendix).

### *2.3 Chronology*

To provide a chronology to constrain the timing of reconstructed RSL changes we use a range of complementary methods to maximise the precision of the resultant age-depth model. Very low concentrations of  $^{210}\text{Pb}$  in the sediments required us to use other methods to provide recent sedimentation rates. We investigated the presence of Total Mercury (Hg) (mg/kg, which includes both mineral and atmospheric deposition) within the sediments using acid dissolution and quadrupole ICP-MS as an indicator of anthropogenic emissions. Other studies in western and northern Greenland note that between 1850-1900 CE there is more than a 2-fold increase in abundance of total Hg in lake sediments compared to late Holocene levels (Bindler et al., 2001; Lindeberg et al., 2006; Shotyk et al., 2003; Zheng, 2015), whereas Perez-Rodriguez et al. (2018) see a rapid increase in Hg abundance from 1880 onwards in southern Greenland. We therefore assume that the onset of detectable Hg above

background level in the Dronning Marie Dal saltmarsh sediments at 4-4.5 cm indicates an age of 1850-1900 CE and use  $1875 \pm 25$  CE in the age-depth modelling described below. For the earlier part of the sediment record we submitted seeds and leaves from saltmarsh and nearby freshwater plants picked from multiple horizons within the sediment for AMS  $^{14}\text{C}$  dating at the  $^{14}\text{Chrono}$  centre at Queen's University, Belfast (Table 1). We generated an age-depth model for the whole sequence using the *P\_Sequence* approach with *variable k* in Oxcal v. 4.3 using the IntCal20 calibration curve (Bronk Ramsey, 2009; Ramsey and Lee, 2013; Reimer et al., 2020). The resultant age-depth model uses the Hg chronohorizon (1850-1900 CE) and three  $^{14}\text{C}$  dates from lower in the sequence to estimate the age of every 0.25 cm of sediment in the sediment section with associated uncertainty (Table A1 and Table A2 in Appendix). The chronological uncertainty reported throughout this study is the 95% probability distribution (Bronk Ramsey, 2009).

We exclude the  $^{14}\text{C}$  ages at 6-6.5 cm (UBA28477) and 9-9.5 cm (UBA28478) from the age-depth model because they were on extremely small samples ( $<0.3$  mg carbon) and are from samples that mix seeds and leaves from high salt marsh with freshwater plants that would not have been growing close together at the time (based on the palaeoenvironment recorded by the fossil diatom assemblage, and the distribution of diatoms and vegetation types on the present-day saltmarsh) (Table 1). The dated macrofossils from lower in the sequence are more likely to be autochthonous as the diatoms record a high marsh to freshwater environment, close to HAT, at the time of deposition.

*Table 1. Radiocarbon dated samples from the Dronning Marie Dal saltmarsh core. Samples at 6-6.5 and 9-9.5 cm are not included in the chronology because they were on extremely small samples ( $<0.3$  mg when graphitized) and mix seeds and leaves from different sources.*

Core depth (cm)	Lab number	<sup>14</sup> C age (yr BP)	<sup>14</sup> C age error (yr/1 sigma)	F <sup>14</sup> C	F <sup>14</sup> C error	Calibrated age yr CE (unmodelled)	Cal curve	Dated material	Used in age model ?
6-6.5	UBA284 77	Modern	n/a	1.02 65	0.142 1	n/a	n/a	Carex subspathacea seeds and Empetrum nigrum leaves	N
9-9.5	UBA284 78	Modern	n/a	1.01 07	0.005 2	n/a	n/a	Carex subspathacea seeds and Empetrum nigrum leaves	N
10-10.5	UBA284 81	208 BP	67	n/a	n/a	1520-1950	INTC AL20	Carex subspathacea seeds	Y
11.5-12	UBA284 76	134 BP	93	n/a	n/a	1528-1950	INTC AL20	Carex subspathacea seeds	Y
12-13	UBA284 79	44 BP	45	0.99 453	0.005 55	1683-1930	INTC AL20 + NHZ 1	Carex subspathacea seeds	Y

271

## 272 2.4 Modelling RSL

### 273 2.4.1 Deglacial RSL change

274 There is a high degree of uncertainty on the rate of GIA in south-east Greenland, owing largely to the  
275 lack of Holocene RSL data points to constrain deglacial history. Marine ingress into an isolation  
276 basin at Timmiarmiut (100 km SW of Dronning Marie Dal) at c. 1140 CE (Table 2, also see Figures  
277 A1, A2 and Table A1 in the Appendix) gives an empirical estimate of regional GIA and suggests that  
278 the linear rate of background RSL change over the past millennium is in the range of +0.2 to +0.8mm/yr  
279 (Table 2). We therefore use a mid-point value of +0.5 mm/yr as the rate of RSL change due to ongoing  
280 deglacial GIA in this study, rather than model predictions outlined in Section 2.1 which are not validated  
281 using RSL data from this region.

282

283 *Table 2. Isolation basin sea-level index point from Timmiarmiut used to calculate the rate of RSL due*  
284 *to ongoing GIA in this study.*

Location (lat,lon)	Sill height (m MTL)	Reference Water Level	RSL (m)	Max cal age CE	Min cal age CE	Cal age error +/-	<sup>14</sup> C age	Lab code
--------------------	---------------------	-----------------------	---------	----------------	----------------	-------------------	---------------------	----------

Timmiarmiut XC1403A (62.4987, - 42.2577)	1.33 +/- 0.5	Ingression (MHWST to HAT)	-0.24 +/- 0.5	1044	1243	99.5	873 +/- 30	AAR 25631
---	-----------------	---------------------------------	------------------	------	------	------	---------------	--------------

285

#### 286 2.4.2 Post Little Ice Age Greenland contribution

287 The post-LIA contribution to RSL at Dronning Marie Dal is computed using the sea level algorithm of  
288 Kendall et al. (2005) computerised by Milne and Mitrovica (2003). This code computes the geoidal and  
289 crustal response to ice and ocean loads on a spherically-symmetric Earth discretized into 25 km-thick  
290 elastic layers as defined by Dziewonski and Anderson (1981), and three viscous layers comprising a  
291 lithosphere, upper and lower mantle. Lithospheric thicknesses (L) in the range 71-120 km are  
292 considered, with upper mantle ( $v_{UM}$ ) and lower mantle ( $v_{LM}$ ) viscosities of  $0.1-1 \times 10^{21}$  and  $1-50 \times 10^{21}$   
293 Pa s explored to quantify the effect on predicted RSL change of different assumptions about Earth  
294 viscosity structure. The post-LIA ice history for the GrIS is derived from Kjeldsen et al. (2015) who  
295 used a collection of aerial imagery from 1978-1987 CE to compare to historical trimlines assumed to  
296 be indicative of a maximum LIA position of the ice sheet and use 1900 CE as a Greenland-wide year  
297 of retreat from the maximum position, while acknowledging considerable local and regional  
298 differences. The extrapolation method of point-scale changes in ice thickness over this time period to  
299 the rest of the Greenland Ice Sheet is detailed in the methods section of Kjeldsen et al. (2015).

300

#### 301 2.4.3 Contribution from Greenland glaciers

302 Changes in ice thickness in peripheral Greenland glaciers is determined in exactly the same way as the  
303 post-LIA Greenland contribution. The peripheral Greenland glacier mass balance history is extracted  
304 from Marzeion et al. (2015) and considered separately from the global glacier dataset (Section 2.4.4)  
305 due to their proximity to the field site; the RSL response is computed as described in Section 2.4.2.

306

#### 307 2.4.4 Contribution from global glaciers

308 We calculate the sea level contribution from global glaciers by first computing the global fingerprint  
309 for a +1mm/yr barystatic contribution from glacier complexes defined in Marzeion et al. (2015, 2012)  
310 since 1902. For the purposes of this calculation, we distribute the mass change across the glacierised  
311 regions equally since the use of a 512 harmonic truncation masks sub 100 km-scale variability in ice

thickness change across regions outside of Greenland. Ice thickness change will vary internally to each glacierised area, but the great distance between southeast Greenland and many of the sources of melt means that the solution is insensitive to spatially inhomogeneous changes in ice thickness within the source regions. Ice thickness changes for each of the global glacier complexes are discretized into decadal loading intervals and the global sea level response is computed using the density configuration in the Preliminary Reference Earth Model (PREM) (Dziewonski and Anderson, 1981). We use a lithospheric thickness of 96 km to represent a global average applied to all glacial sites and omit the viscous component from this calculation. Dronning Marie Dal is proximal to glacier sources in Iceland and Baffin Bay so should display some level of sensitivity to ice loss distribution over these glacierised areas. However, it is in the ‘near field’ with respect to both of these sites, and therefore the use of a more realistic ice loss distribution in these areas (e.g. peripheral thinning) will reduce the relative sea-level rise recorded in southeast Greenland. The influence of low-latitude glaciers is excluded from the sea level fingerprint calculations, as the areas of mass loss are below the spatial resolution of the fingerprinting code. This simplified method produces similar results that of Frederikse et al. (2020).

#### 2.4.5 Contribution from the Antarctic Ice Sheet

Loss of ice mass from either East or West Antarctic Ice Sheets will produce a relatively uniform sea-level change fingerprint over the northern Hemisphere (Bamber and Riva, 2010; Mitrovica et al., 2001). Recent Antarctic Ice Sheet change (1992-present) is relatively well-documented and quantified (Meredith et al., 2019) compared to the period represented by the RSL data in this study. However, a recent study by Frederikse et al. (2020) that applied a Monte Carlo approach to balance the budget of global sea-level rise since 1900 used estimates of 20<sup>th</sup> century Antarctic Ice Sheet mass balance obtained from Adhikari et al. (2018) where the focus of mass loss throughout the 20<sup>th</sup> century is thought to be in the West Antarctic Ice Sheet, amounting to a global sea-level change of  $0.05 \pm 0.04$  mm/yr. We use the resulting ensemble from Frederikse et al.’s (2020) analysis to compute Antarctic Ice Sheet contribution at Dronning Marie Dal.

#### 2.4.6 Contribution from steric changes

To compute the contribution from salinity and temperature changes in the nearby ocean, the Thermodynamic Equation of Sea Water (McDougall and Barker, 2011) (algorithm available here: <https://www.teos-10.org/>) was applied to compute the steric height of the ocean. This uses a suite of proximal monthly temperature-depth and salinity-depth profiles extracted from the CMIP6 database for the ‘historical’ experiments covering the period 1850-2014. The ‘historical’ experiment was chosen to produce timeseries of depth-dependant potential temperature and salinity because the experiment forms part of the principal set of CMIP6 simulations, and the forcing datasets provided to the AOGCMs are consistent with a set of atmospheric and ocean observations (Eyring et al., 2016). We use only one configuration of the variant ID, which relates to initialisation time and procedure, specific model physics and forcing (r1i1p1f1) across all AOGCMs considered (NASA-GISS-E2, CESM2, AWI, CanESM5 and FGOALS). The model output from the CMIP6 database has a spatial resolution in the range of 50-200 km, so we use profiles located within 300 km of Dronning Marie Dal to calculate an average trend in steric height for the nearby ocean. The steric heights are computed to reference depth levels of 500 m, 1000 m, 2000 m and 3000 m. Computing steric heights to different reference levels allow us to determine which depth(s) in the ocean are contributing to steric height variability. Ivchenko et al. (2008) determined that for the North Atlantic for the period 1996-2006, applying a reference level of 1000-1500 m was sufficient to capture steric height variability, although this study provides trends in steric height across the maximum depth level available by each model in the region proximal to Dronning Marie Dal.

#### 2.4.7 Terrestrial Water Storage

To estimate the contribution of changes in terrestrial water storage we utilise the ensemble of timeseries of Frederikse et al. (2020) covering the time-period 1900-2018 CE. This dataset was compiled by including the effects of natural variability in water reservoirs attributed to hemispheric-scale atmospheric and ocean circulation changes (Humphrey and Gudmundsson, 2019), changes in storage from dam building (Chao et al., 2008) and groundwater depletion activities (Döll et al., 2014; Wada et al., 2016).

In the next section the results from the field work, RSL reconstruction and sea-level modelling are then compared to better understand changes in mass balance and RSL over recent centuries in southeast Greenland.

### 3. Results

#### 3.1 Modern diatom assemblages

Diatoms are zoned by elevation across the upper part of the intertidal zone at Dronning Marie Dal, with individual species providing useful information for reconstructing RSL. Above 2.2 m MTL (>0.34 m above HAT) no diatoms were found in surface sediments, probably because the environment is too arid. There is a distinctive assemblage containing *Pinnularia intermedia* (>10 % at HAT, increasing to ~55 % in the highest samples) which ends at ~2.2 m MTL. We use this as a proxy sea level indicator to reconstruct palaeo-marsh surface elevation changes when we find *Pinnularia intermedia* either < 10 %, between 10-20 % and above 20 % in fossil counts (Figures 3A and B and Table A2 in the Appendix). These zones are supplemented at lower elevations by a relatively narrow assemblage zone in the high to low marsh where *Pinnularia intermedia* values are negligible, *Navicula cinta* is >5 % and *Navicula salinarum* is not present (Figure 3A and Table A2 in the Appendix). We find these diatom assemblage zones in every marsh we have studied in southeast and southwest Greenland and use them to reconstruct RSL rather than using a transfer function approach as their precision is as good as or better (*Pinnularia intermedia* is present in >15 marshes between 59° and 69° N in southwest and southeast Greenland with a vertical range of 0.2-0.4 m; unpublished data and Long et al., 2012, 2010; Woodroffe and Long, 2010, 2009). This approach also allows us to consider changes in other parameters (e.g. changes in these species abundance between samples and sediment Loss on Ignition) when producing palaeo-marsh surface elevation estimates.

#### 3.2 Core stratigraphy and biostratigraphy

The core stratigraphy consists of a compacted basal freshwater organic silt-clay, grading upwards into organic high saltmarsh sediments, and then into a slightly silt-rich organic low salt marsh towards the surface, with an increase in LOI values towards the surface (Figure 3B). Diatoms are well preserved in the core and show a trend of falling palaeo-marsh surface elevation upwards from the base of the

sequence as *Pinnularia intermedia* declines and *Navicula cincta* increases in abundance (alongside the absence of low marsh species *Navicula salinarum* which provides additional information about palaeo-marsh surface elevations in this part of the core). In the top 3 cm *Pinnularia intermedia* increases in abundance recording RSL beginning to fall and palaeo-marsh surface elevation increasing (Figure 3B).

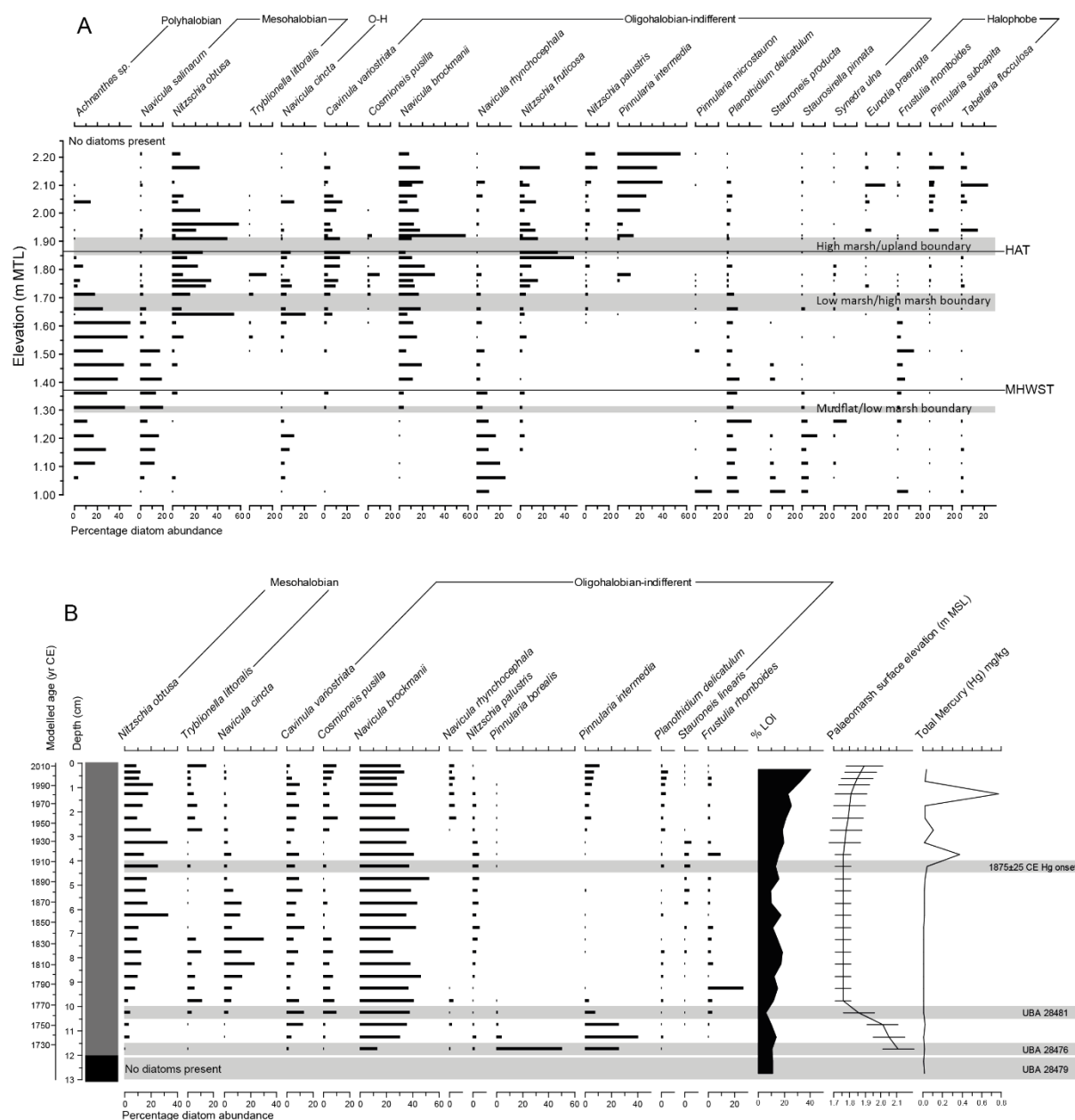


Figure 3. A) Modern diatom data from the marsh at Dronning Marie Dal. Data are expressed as % total diatom valves (%TDV). Only data >10% TDV are shown. B) Fossil diatom counts, palaeo-marsh surface elevation reconstruction and total Mercury measurements from the Dronning Marie Dal saltmarsh core. Diatoms are expressed as a %TDV and only taxa with >10% TDV are shown.



Stratigraphy is shown in lefthand box where grey = saltmarsh sediment, black = freshwater peat. Total

Mercury (mg/kg) was measured on salt marsh sediment using quadrapole ICP-MS.

### 3.3 RSL reconstructions

The saltmarsh sediments and diatoms indicate long term RSL rise. The rate of RSL rise at the start of the record ( $\sim 7$  mm/yr between 1725-1762 CE; Figures 4B and C) is significantly higher than the rate reconstructed from the closest isolation basin at Timmiarmiut ( $+0.5 \pm 0.3$  mm/yr; Table 2). This may be due to LIA ice growth, including the nearby Skinfaxe glacier delivering sediment-laden meltwater to Dronning Marie Dal, causing local ice loading and rapid infilling of accommodation space and salt marsh development. The rate of RSL rise declines rapidly over the period 1762-1880 CE to  $+0.4$  mm/yr and is within the error range of the isolation basin rate during most of this period ( $+0.5 \pm 0.3$  mm/yr). This trend of rapid and then slowly rising RSL between 1725-1880 CE is likely due to changes in the local LIA ice load over this time period combined with ongoing millennial-scale GIA. The HUY3 model predicts  $+1.44$  mm/yr of RSL rise over the past 1000 years in this region (Lecavalier *et al.* 2014) which is larger than but the same sign as the salt marsh and isolation basin RSL data during this period. Other recent estimates of centennial-scale GIA (Khan *et al.*, 2016; van Dam *et al.*, 2017) suggest that RSL should have been falling over the past few hundred years at Dronning Marie Dal. The isolation basin and salt marsh data instead suggest that RSL was rising or close to stable from c. 1100 CE until c. 1880 CE.

Since 1880 CE RSL began to fall, which is indicated clearly in the diatom record by the decline in *Navicula cincta* up core and the reintroduction and increasing abundance of *Pinnularia intermedia*, a high marsh diatom species after 1900 CE (Figure 3B). There is  $\sim 0.09 \pm 0.1$  m of RSL fall since 1880 CE, which if calculated as a constant rate of change is  $-0.72 \pm 1.7$  mm/yr RSL fall (Figures 4B and C, Table 3, Table A2 in the Appendix). Because of the lack of direct dating control in upper part of the core and the slow rate of sedimentation it is not possible to infer decadal changes in RSL rate during the 20<sup>th</sup> Century.

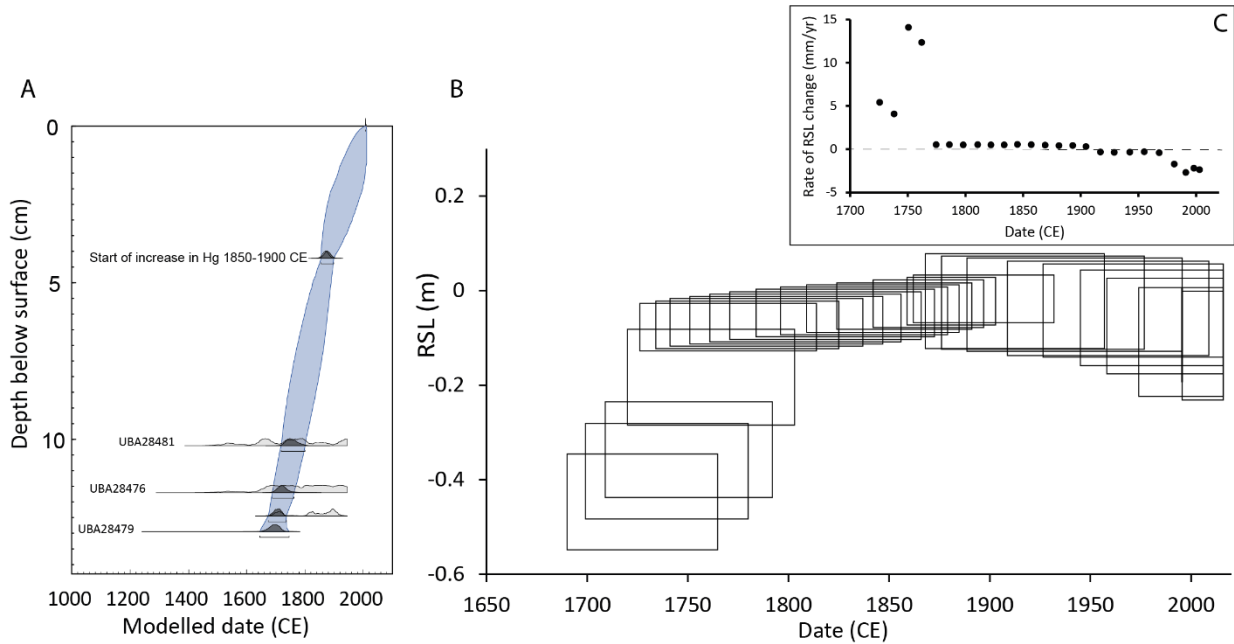


Figure 4A) age-depth model using three  $^{14}\text{C}$  ages and the Hg chrono-horizon, B) Dronning Marie Dal RSL curve, C) rates of RSL change through time inferred from the RSL and age data.

### 3.4 Modelled RSL changes

Published calculations of post LIA Greenland mass loss and other RSL contributors start at 1900 CE (e.g. Kjeldsen et al., 2015; Marzeion et al., 2015), so we focus on this part of the salt marsh RSL record to compare the reconstructed RSL with a modelled sea-level budget. The different contributions to the sea-level budget are summarised in Table 3 and Figure 5. For an average Earth model configuration of  $L = 96\text{km}$ ,  $\nu_{\text{UM}} = 0.5 \times 10^{21} \text{ Pa s}$  and  $\nu_{\text{LM}} = 10 \times 10^{21} \text{ Pa s}$ , post-LIA ice mass loss (from the GrIS only) resulted in sea level change of  $-5.9 \text{ mm/yr}$  at Dronning Marie Dal between 1900-2010 CE. Between 1983-2010 CE the modelled RSL rate was  $-10.1 \text{ mm/yr}$ . Any chosen Earth configuration within the parameter range explored does not significantly affect the predicted sea-level change; for 1900-2010 CE, the range of RSL fall was between  $-6.7$  to  $-5.8 \text{ mm/yr}$  and 1983-2010 CE between  $-11.7$  to  $-9.9 \text{ mm/yr}$ . Using a fixed lithospheric thickness of  $96\text{km}$ , the modelled total sea level fall arising from post-LIA mass loss across a suite of earth models with upper mantle viscosities ranging from  $5 \times 10^{19} - 1 \times 10^{22} \text{ Pa s}$  and lower mantle viscosities in the range of  $1 \times 10^{21} - 5 \times 10^{22} \text{ Pa s}$  was  $0.65$  to  $0.86\text{m}$ , a difference of  $0.21\text{m}$  which is within the uncertainty range of the RSL reconstruction (Figure 4B). The upper mantle viscosity is the largest contribution to this uncertainty accounting for both upper and lower bounds of this range. The effect of reducing the lithospheric thickness from  $120\text{km}$  to  $46\text{km}$  reduces the

amount of modelled relative sea level fall by only a few cm. The contribution of peripheral Greenland glaciers to RSL was on average  $-1.7 \pm 0.2$  mm/yr between 1903 CE and present day; with decadal-scale contributions of -3 to -5 mm/yr between 1923 and 1943 CE. Global glacier mass loss contributes  $+0.24 \pm 0.06$  mm/yr RSL rise between 1903-2009 CE. Antarctica has contributed more significantly to sea-level change in recent years; for the period 1992 to 2016 CE, the Antarctic Peninsula and the West Antarctic Ice Sheet are thought to have resulted in  $+0.06 \pm 0.73$  mm/yr of barystatic sea-level change (Meredith et al., 2019). However, for the period 1850-2014 CE Frederikse et al. (2020) compute  $+0.08 \pm 0.02$  mm/yr, rising to  $+0.2$  mm/yr  $\pm 0.05$  mm/yr between 1970-2018 CE.

The range of values for the modelled steric contribution are in Table 4. They represent an upper estimate of the magnitude and range of the steric component as only profiles showing significant RSL trends are used when calculating the mean. From 1850-2014 CE, trends in steric height are in the range  $-0.23$  to  $+0.18$  mm/yr for a reference depth level of 1000 m and  $-0.36$  to  $+0.28$  mm/yr over a depth range of 2000 m. An observation-based analysis of trends in steric height by Frederikse et al. (2020) shows the steric contribution from the upper 2000m of the ocean close to Dronning Marie Dal between 1957-2018 CE is  $+0.13$  mm/yr (we include steric trends derived for the period 1950-2014 in Table 4 for comparison). All models considered in Table 4 have larger values than Frederikse et al. (2020)'s estimates. Finally, the impact of terrestrial water storage amounts to a sea level fall of  $-0.13 \pm 0.06$  mm/yr at Dronning Marie Dal over the 20<sup>th</sup> century.

The different contributions to RSL are summed and plotted alongside the saltmarsh RSL data in Figure 5. The sum of components predicts RSL fall of between 0.58-0.93 m since 1900 CE. This prediction is dominated by the contribution of GIA caused by post LIA Greenland and peripheral glacier mass loss, which is only counteracted a little by the other components which mostly predict small amounts of RSL rise. The saltmarsh data only reconstruct  $\sim 0.08 \pm 0.1$  m of RSL fall since 1880 CE producing a large mismatch between the sea-level budget and the saltmarsh RSL data.

Table 3. Calculated amounts and rates of RSL change from the various contributors to the RSL budget at Dronning Marie Dal. Rates of RSL change are supplied with  $\pm 2$ -sigma uncertainty unless specified: \* uncertainty reflects assumed  $\pm 10\%$  error on rates which is larger than  $\pm 2$ -sigma. \*\* steric sea level contribution calculated from the average of significant trends for the 0-2000m depth interval from three models in Table 4. \*\*\* GIA from nearby isolation basin ingression with uncertainty calculated from upper and lower elevation reconstruction uncertainties.

Contribution to sea-level budget	Local or global	Time period (CE)	Contribution to RSL change (mm), upper and lower estimates calculated for common period of 1900-2012 CE	Rate of RSL change (mm/yr) assumed for common period of 1900-2012 CE
GIA caused by post LIA ice mass loss*	Local	1900-2010	-724, -593	$-5.9 \pm 0.6$
GIA caused by Greenland peripheral glacier mass change*	Local	1903-2012	-202, -166	$-1.7 \pm 0.2$
Millennial-scale deglacial GIA***	Local	1900-2018	33, 88	$+0.5 \pm 0.3$
<b>Local total</b>				<b><math>-7.1 \pm 0.6</math> mm/yr</b>
Global glaciers	Global	1903-2012	20, 33	$+0.24 \pm 0.06$
Antarctica	Global	1900-2018	0, 18	$+0.08 \pm 0.08$
Steric**	Global	1850-2014	-39, 39	$+0.00 \pm 0.35$
Terrestrial water storage	Global	1900-2018	-21, -8	$-0.13 \pm 0.06$
<b>Global total</b>				<b><math>+0.19 \pm 0.35</math> mm/yr</b>
Total modelled RSL change at Dronning Marie Dal 1900-2012 (see Figure 5)			-933, -589	$-6.9 \pm 1.5$ mm/yr
Rate of RSL change from saltmarsh data (1880-2014)				$-0.72 \pm 1.7$ mm/yr

Table 4: Mean trends in steric height anomalies for three reference levels (500, 1000 and 2000m) calculated from profiles within 300km of Dronning Marie Dal using five models participating in the CMIP6 analysis. In all cases, experiment variant ID was r1i1p1f1. Numbers in brackets denote number of profiles displaying significant trends in steric height from which the mean and 2-sigma trends were calculated. The AWI model produced no significant trends for either time-period whilst GISS-E2 did not produce significant trends for 1850-2014 CE.

Model ID	Resolution (space)	Resolution (time)	0-500m	0-1000m	0-2000m
<b>1850-2014 CE</b>					
GISS-E2	200km	Monthly	-	-	-
CESM2	100km	Monthly	$0.08 \pm 0.01$ (34)	$0.17 \pm 0.01$ (26)	$0.09 \pm 0.01$ (7)
FGOALS	100km	Monthly	$0.14 \pm 0.12$ (7)	$0.18 \pm 0.16$ (11)	$0.28 \pm 0.04$ (6)
AWI	25km	Decadal	-	-	-
CanESM5	100km	Monthly	$-0.12 \pm 0.1$ (13)	$-0.23 \pm 0.08$ (13)	$-0.36 \pm 0.06$ (13)
<b>1950-2014 CE</b>					
GISS_E2	200km	Monthly	$0.17 \pm 0.02$ (10)	$0.36 \pm 0.03$ (6)	$0.75 \pm 0.05$ (3)
CESM2	100km	Monthly	$0.63 \pm 0.15$ (37)	$1.3 \pm 0.11$ (26)	$1.24 \pm 0.07$ (7)
FGOALS	100km	Monthly	$0.43 \pm 0.17$ (11)	$0.57 \pm 0.18$ (12)	$0.81 \pm 0.15$ (6)
AWI	25km	Decadal	-	-	-
CanESM5	100km	Monthly	$0.97 \pm 0.34$ (15)	$1.1 \pm 0.32$ (13)	$0.96 \pm 0.2$ (8)

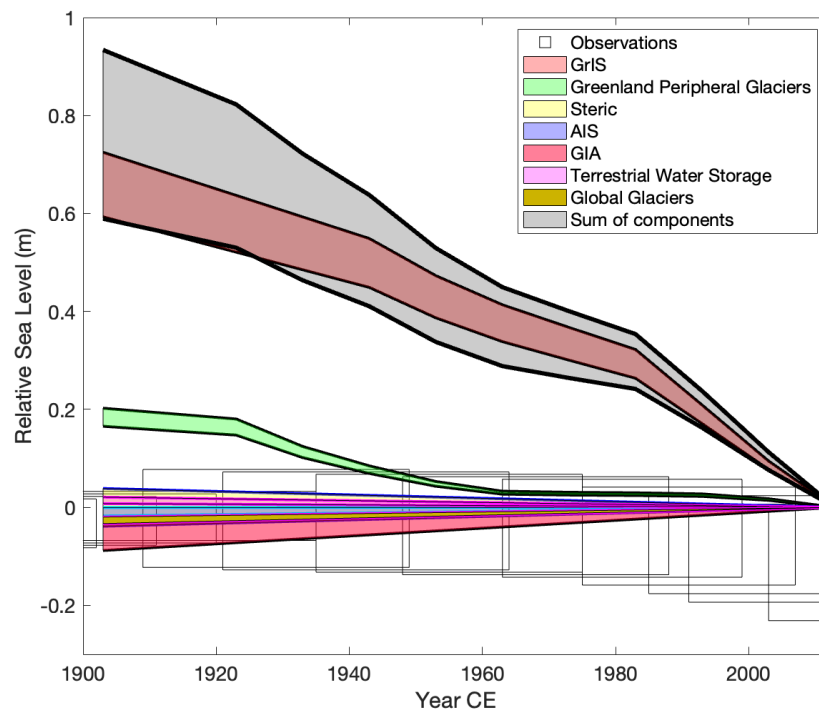


Figure 5: Observed and modelled relative sea level change from 1900-2010 CE as a function of recent and late Holocene Greenland ice thickness changes (GIA caused by the GrIS, Greenland peripheral glaciers and millennial-scale GIA; the 'local' signal) and from sources outside of Greenland (steric signal, AIS, terrestrial water storage and global glaciers). The sum of the modelled components is shown as the grey shaded area and the GrIS and peripheral glacier contributions are shown with an estimated  $\pm 10\%$  uncertainty. The black crosses are the salt marsh-based RSL reconstruction.

## 4. Discussion

The dominant contributors to post-LIA RSL change at Dronning Marie Dal are the adjustment of the solid Earth and changes in geoid height in response to both post-LIA and millennial-scale Greenland ice sheet changes. These contributors (ongoing GIA from the last deglaciation, post LIA Greenland mass balance and mass loss from peripheral Greenland glaciers) amount to a modelled sea-level fall of  $-7.1$  mm/yr between 1900-2010 CE. By contrast, the RSL contributors unrelated to cryospheric change in Greenland only amount to modelled sea-level rise of  $+0.19$  mm/yr, giving a total RSL fall of  $-6.9$  mm/yr between the end of the LIA and present (Table 3). This clearly does not fit with the observations from the salt marsh data (Figures 4B, 5), which suggests that the rate of RSL fall between 1900-2013 CE is  $-0.72 \pm 1.7$  mm/yr.

### 4.1 Timing of the end of the LIA and Greenland ice sheet and peripheral glacier contribution

To try to bring the post-LIA sea-level budget closer to the salt marsh observations, we explore two possible sources of uncertainty in the dominant post LIA Greenland signal: 1) timing of the start of post-LIA mass loss in Greenland and 2) greater uncertainty in modelled sea level associated with post-LIA GrIS and peripheral glacier mass loss.

To explore the possibility that the total post-LIA Greenland mass loss occurred over a longer time period we create five scenarios where the LIA maximum ice termination in Greenland is adjusted to begin at 1700, 1750, 1800, 1850 and 1900 CE, and the rate of mass loss is scaled accordingly with the end point remaining at 2010 (as in Kjeldsen et al., 2015). We know that the LIA ice sheet response was different around Greenland with multiple advance phases forced by different driving mechanisms, and it is simplistic to suggest that the whole of the ice sheet began to lose mass simultaneously at 1900 CE (Kjær et al., 2022), albeit it may serve as a Greenland-wide year. By adjusting the LIA termination date (and therefore the start of Greenland and peripheral glacier mass loss) we can investigate the impact of earlier ice retreat on RSL at Dronning Marie Dal. In this sensitivity analysis we recognise that moving the LIA termination date in our modelling means that we are assuming the LIA ended simultaneously earlier around the whole of Greenland, which is no more nuanced than assuming LIA termination at 1900 CE. We also note that the glaciers closest to Dronning Marie Dal appear to have been at their LIA maximum

position in the early 20<sup>th</sup> Century, which does not agree with an earlier LIA end in this location (Bjork et al., 2012), and a recent alkenone-based sea-surface temperature reconstruction from Nørre Skjoldungesund suggests considerable warming here occurred late, between c. 1915-1945 CE (Wangner et al., 2020). The analysis does however allow a first-order investigation into the sensitivity of modelled post-LIA sea level to the length of time over which the post-LIA mass loss occurred.

The second parameter that we vary as part of this sensitivity study is the total amount of post-LIA RSL change from the GrIS and peripheral glaciers, by assuming an error of up to -30% on these calculations. Kjeldsen et al. 2015 report uncertainties in their mass loss estimates for the Southeast sector of the ice sheet between 7-15 %, and so this sensitivity analysis allows us to test the effect on RSL at Dronning Marie Dal of a smaller amount of mass loss since the end of the LIA in this region.

Varying both LIA termination date and total post LIA mass loss from the GrIS and peripheral glaciers affects how much sea-level change from other components is required to close the post-LIA budget (Figure 6). The ‘budget residual’ in Figure 6 refers to the misfit in mm/yr between the RSL change reconstructed by the saltmarsh data and RSL change predicted by the sea-level budget calculations. In essence this is the amount of sea-level change that we still need to ‘find’ to close the budget even after we modify the timing and total amount of mass loss from the dominant contributors to RSL change of GrIS and peripheral glacier retreat since the end of the LIA.

The time-period over which post LIA mass loss occurs is important for understanding the degree of volume mismatch between the RSL observations and modelled contributions from the maximum extent to present. Figure 6a indicates that moving the LIA termination date from 1900 CE to 1700 CE reduces the ‘budget residual’ required to fit the RSL data from ~+5 to ~+4 mm/yr. This residual is reduced further (to ~+3 mm/yr) when considered alongside a 30% reduction in the amount of RSL fall originating from the GrIS and peripheral glaciers compared to values computed using RSL from ice histories generated by Kjeldsen et al. 2015 (GrIS) and Marzeion et al. 2015 (peripheral glaciers) (Figure 6b). Figures 6c and d further illustrate these results. Figure 6c, where there is no reduction in the amount of post-LIA mass loss shows a poor fit to the RSL data when the LIA termination is moved to

between 1700-1800 CE, and there remains a  $+3.5$  - $5$  mm/yr ‘budget residual’ which must be accounted for from other parts of the sea-level budget. In Figure 6d, a better fit to the RSL data is possible with a 30 % reduction in Greenland and peripheral glacier mass-loss and LIA termination at 1800 CE. The remaining ‘budget residual’ is  $+3$  mm/yr which again must be accounted for from other parts of the sea-level budget.

The smallest calculated ‘budget residual’ ( $\sim +3$  mm/yr) has to be found from processes causing sea-level rise in southeast Greenland, such as millennial-scale Greenland GIA, Antarctic Ice Sheet melt, the steric effect, and global glacier melt. The modelled sea-level budget suggests that these processes are only small contributors to total sea-level change, with the sum of sources from outside Greenland only  $+0.19$  mm/yr since 1900 CE. The steric effect has the largest uncertainty, which we consider in Section 4.8 alongside other potential sources of error in our calculations. It is difficult however to see how the contributors to RSL rise in southeast Greenland could be significantly larger before 1900 CE given the cooler regional temperatures of the LIA.



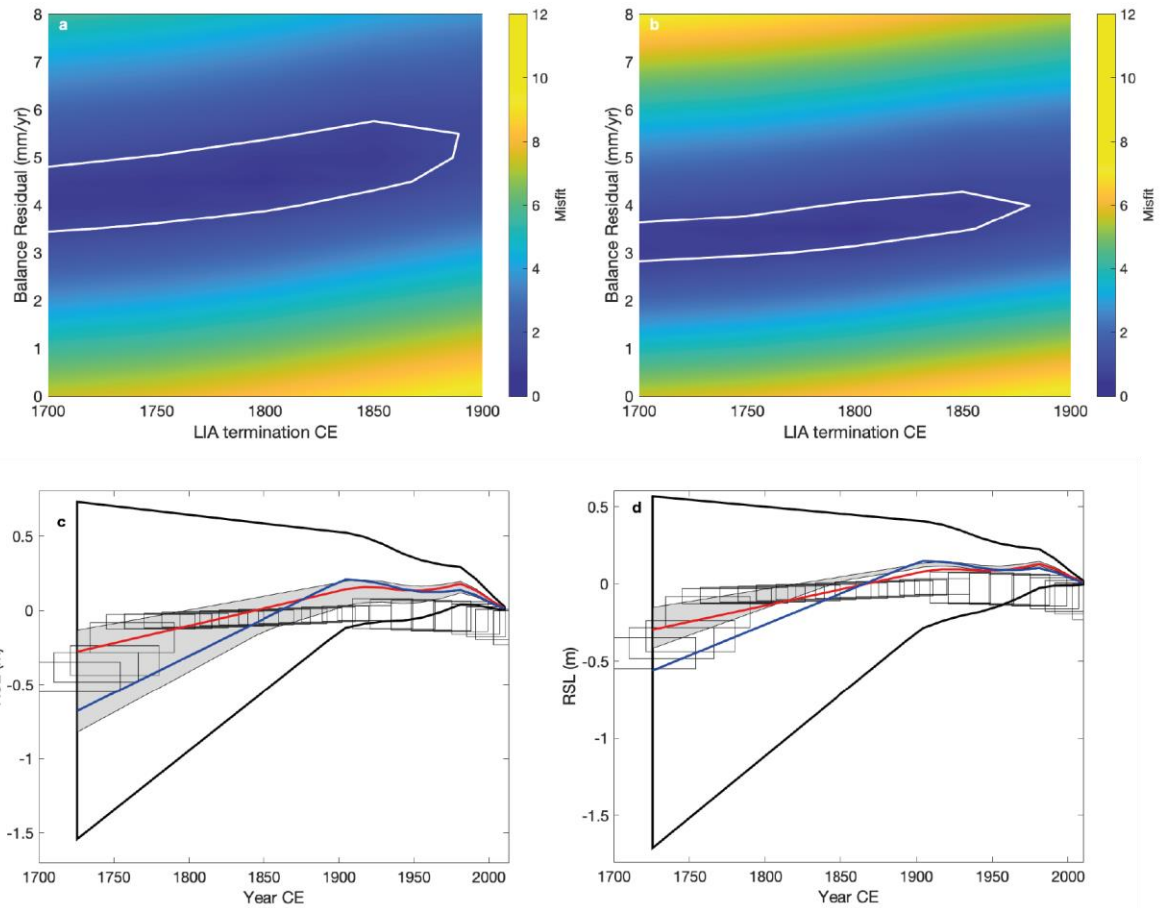


Figure 6. a, b) Misfit plots showing model data-fit where combinations of ‘budget residuals’ and LIA termination dates are considered with (a) no assumed error in the RSL contribution from the GrIS and (b) a 30 % reduction in magnitude of sea-level change associated with local changes in the GrIS. Areas within the white lines have a statistically equivalent fit to the RSL data, c) Modelled RSL from all combinations of LIA termination date and budget residual, assuming no error in the RSL contribution from the GrIS. Area within the black line denotes all possible combinations of RSL trends from LIA terminations from 1750-1900 CE and budget residual rates between 0-6mm/yr. Grey shaded area corresponds to RSL trends from within white lines on Figure 6a, demonstrating a statistically equivalent fit to the data. For illustrative purposes, the red line denotes a modelled RSL scenario with a LIA termination date of 1900 CE (assumed LIA termination date in Kjeldsen et al. 2015) and a budget residual rate of +4mm/yr the blue line a modelled RSL scenario with a budget residual rate of +5mm/yr and LIA termination date of 1900 CE. d) As part c except grey shaded area corresponds to RSL trends from Figure 6b, demonstrating a statistically equivalent fit to the data. For illustrative purposes, the red line denotes a modelled RSL scenario with a budget residual rate of +3mm/yr and LIA termination

date of 1700 CE; the blue line a modelled RSL scenario with a budget residual rate of +4mm/yr and LIA termination date of 1900 CE.

#### 4.2 Reliability of saltmarsh RSL data

Saltmarshes and their microfossil communities are widely used in temperate locations and previously in west and south Greenland to reconstruct recent RSL changes with high precision (e.g. Kemp et al., 2009, 2017; Long et al., 2012, 2010; Woodroffe and Long, 2009). At Dronning Marie Dal, the first half of the RSL record (1725-1880 CE) is harder to interpret because early, rapid RSL rise may indicate either a local LIA loading signal or a non RSL factor (e.g. sediment supply changes) as the marsh became established. What we can say with certainty is that RSL began to fall at or soon after 1880 CE, suggesting additional contributors to RSL or changes in the dominance of existing contributors caused this change in the sign and rate of RSL. We are also confident of the total amount of RSL fall between 1880 CE and present, which is less than predicted by any permutation of the sea-level budget modelling (Figure 5). We acknowledge however that these reconstructions come from a single sediment core and although the stratigraphy appeared consistent across the marsh during fieldwork it would be ideal to replicate these results within another core from the same marsh and also from other marshes close to the ice sheet margin in this region in the future.

There is no indication of hiatuses within the marsh sediment and based on surveys of modern marshes here and elsewhere in Greenland the elevation range of the key diatom species *Pinnularia intermedia* used in the palaeo-marsh surface elevation calculations is robust. A RSL fall of ~0.6-0.9 m since 1900 CE as predicted by the sea-level budget modelling, would have lifted what was a high marsh environment at the start of the period (indicated by the taxa at ~5 cm depth, Figure 3B) out of the intertidal and into the adjacent freshwater zone where diatoms are not preserved due to extreme aridity. The continuous preservation of intertidal diatoms through the sediment sequence to the surface where modern saltmarsh plants were growing during sampling (Figure 2) rules out this possibility. Even the smaller amount of RSL fall (~0.2 m) since 1900 CE predicted by an earlier LIA termination date (1800 CE) and 30% smaller GrIS contribution (Figure 6) is unlikely because the diatoms suggest a mid-high marsh environment at 1900 CE and the core top elevation is within the high marsh zone, a vertical

distance based on analysis of modern diatoms at Dronning Marie Dal of ~0.1 m, which is half of the predicted RSL fall (~0.2 m). Greenland saltmarshes accrete very slowly and only record sustained RSL changes over decades, and therefore short-timescale variability in contributors (e.g. due to decadal temperature fluctuations in the 20<sup>th</sup> Century) is not distinguishable in the saltmarsh data. However, the total amount of RSL fall and the timing of the change from RSL rise/stability to RSL fall is robustly reconstructed and we are confident that this provides an important test of Greenland RSL modelling.

#### *4.3 Limitations of RSL modelling*

Regional sea level budgets deviate significantly from the global budget, are challenging to compute and have been deemed part of the ‘Regional Sea-Level Change and Coastal Impacts’ Grand Challenge by the World Climate Research Programme (WCRP, 2022). Of the different items in the sea-level budget for Dronning Marie Dal, the large uncertainty in the steric contribution could potentially be the source of additional sea-level rise which would help decrease the ‘budget residual’ identified in Figure 6. The data in Table 4 do not fully capture the range of uncertainty in the steric component of sea level. These uncertainties arise from poor to non-existent capture of the dynamics of coastal regions, namely the propagation of the change in steric height of the open ocean to the fjord location and the lack of observations to constrain model output in the early 20<sup>th</sup> Century.

The field site is located at the head of the 50 km long marine fjord Søndre Skoldungesund and therefore the steric contribution may be different to that calculated from the open ocean estimates within 300 km of Dronning Marie Dal averaged in this study. A multibeam study of the fjord by Kjeldsen et al. (2017) shows the fjord is between 1.1-3.1 km wide, up to 800 m deep in the outer part, with a shallow (77m deep) sill at mid-fjord and shallow depths inside the sill. The fjord water is cold to the base along its length, with no apparent intrusion of warmer Atlantic water from the shelf edge. The mixed predictions of steric height changes from the different models suggest that this region is poorly constrained within global steric datasets (Table 4). Given the lack of intrusion of warm Atlantic water into the fjord today it is unlikely that there has been a more positive contribution of steric height from 20<sup>th</sup> Century warming. However, with significant mass loss from the Greenland Ice Sheet since the LIA and an influx of cold

yet low-salinity meltwater into the fjord it is possible that the local halosteric component is underestimated.

A second issue with the steric height calculation is the potential for the CMIP6 models to misrepresent changes in the dynamic height of the ocean caused by shifts in the location of ocean currents, such as the East Greenland Current (EGC) over time. A recent study of North Atlantic dynamic sea level and its response to GrIS meltwater and temperature increase indicates general Atlantic Meridional Overturning Circulation decline and increase in sea-surface height with increased GrIS melting, but the response of the cold EGC is complex and in southeast Greenland the effect of warming and increased meltwater on sea-surface height is minimal (Saenko et al., 2017). Given that Kjeldsen et al. (2017) suggest the EGC does not currently penetrate into the Søndre Skoldungesund fjord the impact of any dynamical changes in the EGC since the LIA are likely to be minor.

A third possible source of uncertainty in the sea-level budget is the application of the sea level code used to calculate GIA, specifically the spectral resolution with which the algorithm predicts the sea level response to loading increments. The mass balance history from Kjeldsen et al. (2015) is presented on a 1x1 km spatial grid, but the sea level code utilises a spectral harmonic truncation of 256. The effects on predicted RSL of the reduction in resolution has been demonstrated previously with near-field relative sea level being more affected by harmonic truncation than far field sites (Spada and Melini, 2019). A move towards a higher degree spherical harmonic truncation (>1024) would be necessary to faithfully reproduce sea level fingerprint histories associated with small outlet glaciers and should be considered in the future (Adhikari et al., 2015).

Despite the limitations outlined above, this study presents a first test of a post-LIA sea-level budget in the nearfield location of southeast Greenland. There is clear and unexplained difference between the RSL history recorded by salt marsh sediments (a small RSL fall since the end of the LIA) and the RSL budget which suggests significant RSL fall during this period. The sensitivity tests show that the budget can fit the salt marsh RSL data if the amount of mass loss from the GrIS and peripheral glaciers is less, and it took place over a longer period (Figure 6d), but even so a +2.5 mm/yr unexplained ‘budget

residual' remains. RSL reconstructions from salt marshes in southwest Greenland (Long et al., 2012, 2010; Woodroffe and Long, 2010, 2009) also suggest that the dominant signal in southern Greenland is RSL rise into the 20<sup>th</sup> Century, which correlates with the long term (pre ~1880 CE) trend of RSL rise at Dronning Marie Dal.

## 5. Conclusions

Saltmarsh sediments collected at the mouth of Dronning Marie Dal, close to the GrIS margin in southeast Greenland, record RSL changes over the past c. 300 years in changing sediment and diatom stratigraphy. These RSL changes record a combination of processes that are dominated by local/regional changes in GrIS mass balance during this critical period that spans the maximum of the LIA and 20th Century warming.

In the early part of the record (1725-1762 CE) the rate of RSL rise is higher than reconstructed from the closest isolation basin at Timmiarmiut, but between 1762-1880 CE the rate decreases to within the error range of the isolation basin RSL rate. This trend is likely due to changes in the local LIA ice load over this time-period combined with ongoing millennial-scale GIA, or other local processes as the salt marsh is established. Other recent estimates of centennial-scale GIA (Khan et al., 2016; van Dam et al., 2017) suggest that RSL should have been falling over the past few hundred years at Dronning Marie Dal. The isolation basin and salt marsh data instead suggest that RSL was rising or close to stable from c. 1100 CE until c. 1880 CE. RSL begins to slowly fall around 1880 CE, with a total amount of RSL fall of  $0.09 \pm 0.1$  m since 1880 CE.

Modelled RSL, which takes into account contributions from post-LIA GrIS GIA, ongoing deglacial GIA, the global non-ice sheet glacial fingerprint, the contribution from thermosteric effects, an estimate of the Antarctic fingerprint and the contribution from terrestrial water storage, over-predicts the amount of RSL fall since the end of the LIA by at least 0.5 m. The GIA signal caused by post-LIA GrIS mass loss is by far the largest contributor, and error in its calculation has the largest potential to impact RSL predictions at Dronning Marie Dal. We cannot reconcile the modelled contributions and the saltmarsh observations, even when moving the termination of the LIA to 1700 CE, and reducing the post-LIA

Greenland mass loss signal by 30%. A ‘budget residual’ of  $\sim +3$  mm/yr since the end of the LIA remains unexplained. Explaining the difference between salt marsh RSL data and the modelled RSL budget since the end of the LIA and determining the timing of the LIA termination should be a key future research objectives which can be addressed through reducing uncertainty on each component to the sea-level budget, collecting more empirical data on the recent history of the GrIS and by replicating the salt marsh RSL record presented here elsewhere in this and other regions of Greenland.

#### *Author Contribution*

SAW, LMW, AJL and KKK designed the study, SAW, KKK and KHK undertook fieldwork, NLMB undertook the laboratory analysis, and SAW and LMW prepared the manuscript with contributions from all co-authors.

The authors declare that they have no conflict of interest.

#### *Acknowledgements*

We acknowledge funding from Danish Agency for Science, Technology and Innovation, ‘Greenland ice sheet over the past millennium’ (PI Kurt Kjær) and the assistance of the captain and crew onboard SS ACTIV for their help collecting the data during the field campaign to southeast Greenland. Barlow’s postdoctoral position to undertake this work was funded by Durham University Department of Geography. We thank the laboratory technicians within Durham Geography for their support with sample preparation. We thank Dr Robin Edwards and Dr Udit Mukherjee for their insightful comments which improved an earlier version of this manuscript. The authors acknowledge the International Union for Quaternary Sciences (INQUA) Coastal and Marine Processes (CMP) Commission and PALSEA, a working group of INQUA and Past Global Changes (PAGES), which in turn receives support from the Swiss Academy of Sciences and the Chinese Academy of Sciences.

Adhikari, S., Ivins, E. R., and Larour, E.: ISSM-SESAW v1.0: mesh-based computation of gravitationally consistent sea level and geodetic signatures caused by cryosphere and climate driven mass change, *Climate and Earth System Modeling*, <https://doi.org/10.5194/gmdd-8-9769-2015>, 2015.

- 741 Adhikari, S., Caron, L., Steinberger, B., Reager, J. T., Kjeldsen, K. K., Marzeion, B., Larour,  
742 E., and Ivins, E. R.: What drives 20th century polar motion?, *Earth Planet. Sci. Lett.*, 502,  
743 126–132, <https://doi.org/10.1016/j.epsl.2018.08.059>, 2018.
- 744 Adhikari, S., Milne, G. A., Caron, L., Khan, S. A., Kjeldsen, K. K., Nilsson, J., Larour, E., and  
745 Ivins, E. R.: Decadal to Centennial Timescale Mantle Viscosity Inferred from Modern Crustal  
746 Uplift Rates in Greenland, *Geophys. Res. Lett.*, n/a, e2021GL094040,  
747 <https://doi.org/10.1029/2021GL094040>, 2021.
- 748 Allen, J. R. L.: Morphodynamics of Holocene salt marshes: a review sketch from the Atlantic  
749 and Southern North Sea coasts of Europe, *Quat. Sci. Rev.*, 19, 1155–1231,  
750 [https://doi.org/10.1016/S0277-3791\(99\)00034-7](https://doi.org/10.1016/S0277-3791(99)00034-7), 2000.
- 751 Bamber, J. and Riva, R.: The sea level fingerprint of recent ice mass fluxes, *The*  
752 *Cryosphere*, 4, 621–627, <https://doi.org/10.5194/tc-4-621-2010>, 2010.
- 753 Barlow, N. L. M., Shennan, I., Long, A. J., Gehrels, W. R., Saher, M. H., Woodroffe, S. A.,  
754 and Hillier, C.: Salt marshes as late Holocene tide gauges, *Glob. Planet. Change*, 106, 90–  
755 110, <https://doi.org/10.1016/j.gloplacha.2013.03.003>, 2013.
- 756 Bevis, M., Wahr, J., Khan, S. A., Madsen, F. B., Brown, A., Willis, M., Kendrick, E., Knudsen,  
757 P., Box, J. E., van Dam, T., Caccamise, D. J., Johns, B., Nylen, T., Abbott, R., White, S.,  
758 Miner, J., Forsberg, R., Zhou, H., Wang, J., Wilson, T., Bromwich, D., and Francis, O.:  
759 Bedrock displacements in Greenland manifest ice mass variations, climate cycles and  
760 climate change, *Proc. Natl. Acad. Sci. U. S. A.*, 109, 11944–11948, [https://doi.org/DOI](https://doi.org/10.1073/pnas.1204664109)  
761 [10.1073/pnas.1204664109](https://doi.org/10.1073/pnas.1204664109), 2012.
- 762 Bevis, M., Harig, C., Khan, S. A., Brown, A., Simons, F. J., Willis, M., Fettweis, X., Broeke,  
763 M. R. van den, Madsen, F. B., Kendrick, E., Caccamise, D. J., Dam, T. van, Knudsen, P.,  
764 and Nylen, T.: Accelerating changes in ice mass within Greenland, and the ice sheet's  
765 sensitivity to atmospheric forcing, *Proc. Natl. Acad. Sci.*, 116, 1934–1939,  
766 <https://doi.org/10.1073/pnas.1806562116>, 2019.
- 767 Bindler, R., Renberg, I., Appleby, P. G., Anderson, N. J., and Rose, N. L.: Mercury  
768 Accumulation Rates and Spatial Patterns in Lake Sediments from West Greenland: A Coast  
769 to Ice Margin Transect, *Environ. Sci. Technol.*, 35, 1736–1741,  
770 <https://doi.org/10.1021/es0002868>, 2001.
- 771 Bjork, A. A., Kjaer, K. H., Korsgaard, N. J., Khan, S. A., Kjeldsen, K. K., Andresen, C. S.,  
772 Box, J. E., Larsen, N. K., and Funder, S.: An aerial view of 80 years of climate-related glacier  
773 fluctuations in southeast Greenland, *Nat. Geosci.*, 5, 427–432,  
774 <https://doi.org/10.1038/Ngeo1481>, 2012.
- 775 Briner, J. P., Young, N. E., Thomas, E. K., Stewart, H. A. M., Losee, S., and Truex, S.: Varve  
776 and radiocarbon dating support the rapid advance of Jakobshavn Isbræ during the Little Ice  
777 Age, *Quat. Sci. Rev.*, 30, 2476–2486, <https://doi.org/10.1016/j.quascirev.2011.05.017>, 2011.
- 778 Briner, J. P., Cuzzone, J. K., Badgley, J. A., Young, N. E., Steig, E. J., Morlighem, M.,  
779 Schlegel, N.-J., Hakim, G. J., Schaefer, J. M., Johnson, J. V., Lesnek, A. J., Thomas, E. K.,  
780 Allan, E., Bennike, O., Cluett, A. A., Csatho, B., de Vernal, A., Downs, J., Larour, E., and  
781 Nowicki, S.: Rate of mass loss from the Greenland Ice Sheet will exceed Holocene values  
782 this century, *Nature*, 586, 70–74, <https://doi.org/10.1038/s41586-020-2742-6>, 2020.
- 783 van den Broeke, M., Bamber, J., Ettema, J., Rignot, E., Schrama, E., van de Berg, W., van  
784 Meijgaard, E., Velicogna, I., and Wouters, B.: Partitioning Recent Greenland Mass Loss,  
785 *Science*, 326, 984–986, <https://doi.org/10.1126/science.1178176>, 2009.

786 Bronk Ramsey, C.: Bayesian analysis of radiocarbon dates, *Radiocarbon*, 51, 337–360,  
787 2009.

788 Chao, B. F., Wu, Y. H., and Li, Y. S.: Impact of Artificial Reservoir Water Impoundment on  
789 Global Sea Level, *Science*, 320, 212–214, <https://doi.org/10.1126/science.1154580>, 2008.

790 Chen, G., Zhang, S., Liang, S., and Zhu, J.: Elevation and Volume Changes in Greenland  
791 Ice Sheet From 2010 to 2019 Derived From Altimetry Data, *Front. Earth Sci.*, 9, 674983,  
792 <https://doi.org/10.3389/feart.2021.674983>, 2021.

793 Chylek, P., Dubey, M. K., and Lesins, G.: Greenland warming of 1920-1930 and 1995-2005,  
794 *Geophys. Res. Lett.*, 33, <https://doi.org/Artn L11707> 10.1029/2006gl026510, 2006.

795 van Dam, T., Francis, O., Wahr, J., Khan, S. A., Bevis, M., and van den Broeke, M. R.: Using  
796 GPS and absolute gravity observations to separate the effects of present-day and  
797 Pleistocene ice-mass changes in South East Greenland, *Earth Planet. Sci. Lett.*, 459, 127–  
798 135, <https://doi.org/10.1016/j.epsl.2016.11.014>, 2017.

799 Döll, P., Müller Schmied, H., Schuh, C., Portmann, F. T., and Eicker, A.: Global-scale  
800 assessment of groundwater depletion and related groundwater abstractions: Combining  
801 hydrological modeling with information from well observations and GRACE satellites, *Water*  
802 *Resour. Res.*, 50, 5698–5720, <https://doi.org/10.1002/2014WR015595>, 2014.

803 Dyke, L. M., Hughes, A. L. C., Murray, T., Hiemstra, J. F., Andresen, C. S., and Rodés, Á.:  
804 Evidence for the asynchronous retreat of large outlet glaciers in southeast Greenland at the  
805 end of the last glaciation, *Quat. Sci. Rev.*, 99, 244–259,  
806 <https://doi.org/10.1016/j.quascirev.2014.06.001>, 2014.

807 Dyke, L. M., Hughes, A. L., Andresen, C. S., Murray, T., Hiemstra, J. F., Bjørk, A. A., and  
808 Rodés, Á.: The deglaciation of coastal areas of southeast Greenland, *The Holocene*, 28,  
809 1535–1544, <https://doi.org/10.1177/0959683618777067>, 2018.

810 Dziewonski, A. M. and Anderson, D. L.: Preliminary reference Earth model, *Phys. Earth*  
811 *Planet. Inter.*, 25, 297–356, [https://doi.org/10.1016/0031-9201\(81\)90046-7](https://doi.org/10.1016/0031-9201(81)90046-7), 1981.

812 Eyring, V., Bony, S., Meehl, G. A., Senior, C. A., Stevens, B., Stouffer, R. J., and Taylor, K.  
813 E.: Overview of the Coupled Model Intercomparison Project Phase 6 (CMIP6) experimental  
814 design and organization, *Geosci. Model Dev.*, 9, 1937–1958, [https://doi.org/10.5194/gmd-9-](https://doi.org/10.5194/gmd-9-1937-2016)  
815 1937-2016, 2016.

816 Farrell, W. E. and Clark, J. A.: On Postglacial Sea Level, *Geophys. J. R. Astron. Soc.*, 46,  
817 647–667, <https://doi.org/10.1111/j.1365-246X.1976.tb01252.x>, 1976.

818 Frederikse, T., Landerer, F., Caron, L., Adhikari, S., Parkes, D., Humphrey, V. W.,  
819 Dangendorf, S., Hogarth, P., Zanna, L., Cheng, L., and Wu, Y.-H.: The causes of sea-level  
820 rise since 1900, *Nature*, 584, 393–397, <https://doi.org/10.1038/s41586-020-2591-3>, 2020.

821 Funder, S. and Hansen, L.: The Greenland ice sheet - a model for its culmination and decay  
822 during and after the last glacial maximum, *Bull. Geol. Soc. Den.*, 42, 137–152, 1996.

823 Funder, S., Kjeldsen, K. K., Kjaer, K. H., and O Cofaigh, C.: The Greenland Ice Sheet during  
824 the last 300,000 years: a review, *Dev. Quat. Sci.*, 15, 699-713. doi: 10.1016/B978-0-444-  
825 53447-7.00050-7, 2011.

826 Hughes, A., Rainsley, E., Murray, T., Fogwill, C., Schnabel, C., and Xu, S.: Rapid response  
827 of Helheim Glacier, southeast Greenland, to early Holocene climate warming, *Geology*, 40,  
828 427–430, <https://doi.org/10.1130/G32730.1>, 2012.



829 Humphrey, V. and Gudmundsson, L.: GRACE-REC: a reconstruction of climate-driven water  
830 storage changes over the last century, *Earth Syst. Sci. Data*, 11, 1153–1170,  
831 <https://doi.org/10.5194/essd-11-1153-2019>, 2019.

832 Ivchenko, V. O., Danilov, S., Sidorenko, D., Schröter, J., Wenzel, M., and Aleynik, D. L.:  
833 Steric height variability in the Northern Atlantic on seasonal and interannual scales, *J.*  
834 *Geophys. Res.*, 113, C11007, <https://doi.org/10.1029/2008JC004836>, 2008.

835 Kemp, A., Horton, B., Culver, S., Corbett, D., van de Plassche, O., Gehrels, W., Douglas, B.,  
836 and Parnell, A.: Timing and magnitude of recent accelerated sea-level rise (North Carolina,  
837 United States), *Geology*, 37, 1035–1038, <https://doi.org/10.1130/G30352A.1>, 2009.

838 Kemp, A. C., Kegel, J. J., Culver, S. J., Barber, D. C., Mallinson, D. J., Leorri, E., Bernhardt,  
839 C. E., Cahill, N., Riggs, S. R., Woodson, A. L., Mulligan, R. P., and Horton, B. P.: Extended  
840 late Holocene relative sea-level histories for North Carolina, USA, *Quat. Sci. Rev.*, 160, 13–  
841 30, <https://doi.org/10.1016/j.quascirev.2017.01.012>, 2017.

842 Kendall, R. A., Mitrovica, J. X., and Milne, G. A.: On post-glacial sea level - II. Numerical  
843 formulation and comparative results on spherically symmetric models, *Geophys. J. Int.*, 161,  
844 679–706, <https://doi.org/10.1111/j.1365-246X.2005.02553.x>, 2005.

845 Khan, S. A., Aschwanden, A., Bjork, A. A., Wahr, J., Kjeldsen, K. K., and Kjaer, K. H.:  
846 Greenland ice sheet mass balance: a review, *Rep. Prog. Phys.*, 78, 26,  
847 <https://doi.org/10.1088/0034-4885/78/4/046801>, 2015.

848 Khan, S. A., Sasgen, I., Bevis, M., van Dam, T., Bamber, J. L., Wahr, J., Willis, M., Kjaer, K.  
849 H., Wouters, B., Helm, V., Csatho, B., Fleming, K., Bjork, A. A., Aschwanden, A., Knudsen,  
850 P., and Munneke, P. K.: Geodetic measurements reveal similarities between post-Last  
851 Glacial Maximum and present-day mass loss from the Greenland ice sheet, *Sci. Adv.*, 2,  
852 <https://doi.org/ARTN e1600931> 10.1126/sciadv.1600931, 2016.

853 Khan, S. A., Bjørk, A. A., Bamber, J. L., Morlighem, M., Bevis, M., Kjær, K. H., Mouginot, J.,  
854 Løkkegaard, A., Holland, D. M., Aschwanden, A., Zhang, B., Helm, V., Korsgaard, N. J.,  
855 Colgan, W., Larsen, N. K., Liu, L., Hansen, K., Barletta, V., Dahl-Jensen, T. S.,  
856 Søndergaard, A. S., Csatho, B. M., Sasgen, I., Box, J., and Schenk, T.: Centennial response  
857 of Greenland's three largest outlet glaciers, *Nat. Commun.*, 11, 5718,  
858 <https://doi.org/10.1038/s41467-020-19580-5>, 2020.

859 Kjær, K. H., Bjørk, A. A., Kjeldsen, K. K., Hansen, E. S., Andresen, C. S., Siggaard-  
860 Andersen, M.-L., Khan, S. A., Søndergaard, A. S., Colgan, W., Schomacker, A., Woodroffe,  
861 S., Funder, S., Rouillard, A., Jensen, J. F., and Larsen, N. K.: Glacier response to the Little  
862 Ice Age during the Neoglacial cooling in Greenland, *Earth-Sci. Rev.*, 227, 103984,  
863 <https://doi.org/10.1016/j.earscirev.2022.103984>, 2022.

864 Kjeldsen, K., Korsgaard, N., Bjork, A., Khan, S., Box, J., Funder, S., Larsen, N., Bamber, J.,  
865 Colgan, W., van den Broeke, M., Siggaard-Andersen, M., Nuth, C., Schomacker, A.,  
866 Andresen, C., Willerslev, E., and Kjaer, K.: Spatial and temporal distribution of mass loss  
867 from the Greenland Ice Sheet since AD 1900, *Nature*, 528, 396–400,  
868 <https://doi.org/10.1038/nature16183>, 2015.

869 Kjeldsen, K. K., Weinrebe, R. W., Bendtsen, J., Bjørk, A. A., and Kjær, K. H.: Multibeam  
870 bathymetry and CTD measurements in two fjord systems in southeastern Greenland, *Earth*  
871 *Syst. Sci. Data*, 9, 589–600, <https://doi.org/10.5194/essd-9-589-2017>, 2017.

872 Lecavalier, B., Milne, G. A., Simpson, M. J. R., Wake, L. M., Huybrechts, P., Tarasov, L.,  
873 Kjeldsen, K. K., Funder, S. V., Long, A. J., Woodroffe, S. A., Dyke, A., and Larsen, N. K.: A  
874 model of Greenland ice sheet deglaciation based on observations of relative sea-level and  
875 ice extent, *Quat. Sci. Rev.*, in press, 2014.

- 876 Lepping, O. and Daniëls, F. J. A.: Phytosociology of Beach and Salt Marsh Vegetation in  
877 Northern West Greenland, *Polarforschung*, 76, 95–108, 2007.
- 878 Levy, L. B., Larsen, N. K., Knudsen, M. F., Egholm, D. L., Bjørk, A. A., Kjeldsen, K. K., Kelly,  
879 M. A., Howley, J. A., Olsen, J., Tikhomirov, D., Zimmerman, S. R. H., and Kjær, K. H.: Multi-  
880 phased deglaciation of south and southeast Greenland controlled by climate and  
881 topographic setting, *Quat. Sci. Rev.*, 242, 106454,  
882 <https://doi.org/10.1016/j.quascirev.2020.106454>, 2020.
- 883 Lindeberg, C., Bindler, R., Renberg, I., Emteryd, O., Karlsson, E., and Anderson, N. J.:  
884 Natural Fluctuations of Mercury and Lead in Greenland Lake Sediments, *Environ. Sci.*  
885 *Technol.*, 40, 90–95, <https://doi.org/10.1021/es051223y>, 2006.
- 886 Long, A. J., Woodroffe, S. A., Milne, G. A., Bryant, C. L., and Wake, L. M.: Relative sea-level  
887 change in West Greenland during the last millennium, *Quat. Sci. Rev.*, 29, 367–383, 2010.
- 888 Long, A. J., Woodroffe, S. A., Milne, G. A., Bryant, C. L., Simpson, M. J. R., and Wake, L.  
889 M.: Relative sea-level change in Greenland during the last 700 yrs and ice sheet response to  
890 the Little Ice Age, *Earth Planet. Sci. Lett.*, 315, 76–85, <https://doi.org/DOI>  
891 [10.1016/j.epsl.2011.06.027](https://doi.org/10.1016/j.epsl.2011.06.027), 2012.
- 892 Marzeion, B., Jarosch, A. H., and Hofer, M.: Past and future sea-level change from the  
893 surface mass balance of glaciers, *The Cryosphere*, 6, 1295–1322, [https://doi.org/10.5194/tc-](https://doi.org/10.5194/tc-6-1295-2012)  
894 [6-1295-2012](https://doi.org/10.5194/tc-6-1295-2012), 2012.
- 895 Marzeion, B., Leclercq, P. W., Cogley, J. G., and Jarosch, A. H.: Brief Communication:  
896 Global reconstructions of glacier mass change during the 20th century are consistent, *The*  
897 *Cryosphere*, 9, 2399–2404, <https://doi.org/10.5194/tc-9-2399-2015>, 2015.
- 898 McDougall, T. J. and Barker, P. M.: Getting started with TEOS-10 and the Gibbs Seawater  
899 (GSW) Oceanographic Toolbox., 2011.
- 900 Meredith, M., Sommerkorn, M., Cassotta, S., Derksen, C., Ekaykin, A., Hollowed, A.,  
901 Kofinas, G., Mackintosh, A., Melbourne-Thomas, J., Muelbert, M. M. C., Ottersen, G.,  
902 Pritchard, H., and Schuur, E. A. G.: Polar Regions, in: IPCC Special Report on the Ocean  
903 and Cryosphere in a Changing Climate, Cambridge University Press, 203–320, 2019.
- 904 Mitrovica, J. X. and Milne, G. A.: On post-glacial sea level: I. General theory, *Geophys. J.*  
905 *Int.*, 154, 253–267, <https://doi.org/DOI> [10.1046/j.1365-246X.2003.01942.x](https://doi.org/10.1046/j.1365-246X.2003.01942.x), 2003.
- 906 Mitrovica, J. X., Tamisiea, M. E., Davis, J. L., and Milne, G. A.: Recent mass balance of  
907 polar ice sheets inferred from patterns of global sea-level change, *Nature*, 409, 1026–1029,  
908 <https://doi.org/10.1038/35059054>, 2001.
- 909 Moon, T., Joughin, I., Smith, B., and Howat, I.: 21st-Century Evolution of Greenland Outlet  
910 Glacier Velocities, *Science*, 336, 576–578, <https://doi.org/10.1126/science.1219985>, 2012.
- 911 Morlighem, M., Williams, C. N., Rignot, E., An, L., Arndt, J. E., Bamber, J. L., Catania, G.,  
912 Chauché, N., Dowdeswell, J. A., Dorschel, B., Fenty, I., Hogan, K., Howat, I., Hubbard, A.,  
913 Jakobsson, M., Jordan, T. M., Kjeldsen, K. K., Millan, R., Mayer, L., Mouginot, J., Noël, B. P.  
914 Y., O’Cofaigh, C., Palmer, S., Rysgaard, S., Seroussi, H., Siegert, M. J., Slabon, P., Straneo,  
915 F., van den Broeke, M. R., Weinrebe, W., Wood, M., and Zinglensen, K. B.: BedMachine v3:  
916 Complete Bed Topography and Ocean Bathymetry Mapping of Greenland From Multibeam  
917 Echo Sounding Combined With Mass Conservation, *Geophys. Res. Lett.*, 44, 11,051-  
918 11,061, <https://doi.org/10.1002/2017GL074954>, 2017.
- 919 Pérez-Rodríguez, M., Silva-Sánchez, N., Kylander, M. E., Bindler, R., Mighall, T. M.,  
920 Schofield, J. E., Edwards, K. J., and Martínez Cortizas, A.: Industrial-era lead and mercury

- 921 contamination in southern Greenland implicates North American sources, *Sci. Total*  
922 *Environ.*, 613–614, 919–930, <https://doi.org/10.1016/j.scitotenv.2017.09.041>, 2018.
- 923 Pritchard, H., Arthern, R., Vaughan, D., and Edwards, L.: Extensive dynamic thinning on the  
924 margins of the Greenland and Antarctic ice sheets, *Nature*, 461, 971–975,  
925 <https://doi.org/10.1038/nature08471>, 2009.
- 926 Ramsey, C. B. and Lee, S.: Recent and Planned Developments of the Program OxCal,  
927 *Radiocarbon*, 55, 720–730, <https://doi.org/10.1017/S0033822200057878>, 2013.
- 928 Reimer, P. J., Austin, W. E. N., Bard, E., Bayliss, A., Blackwell, P. G., Ramsey, C. B., Butzin,  
929 M., Cheng, H., Edwards, R. L., Friedrich, M., Grootes, P. M., Guilderson, T. P., Hajdas, I.,  
930 Heaton, T. J., Hogg, A. G., Hughen, K. A., Kromer, B., Manning, S. W., Muscheler, R.,  
931 Palmer, J. G., Pearson, C., Plicht, J. van der, Reimer, R. W., Richards, D. A., Scott, E. M.,  
932 Southon, J. R., Turney, C. S. M., Wacker, L., Adolphi, F., Büntgen, U., Capano, M., Fahrni,  
933 S. M., Fogtmann-Schulz, A., Friedrich, R., Köhler, P., Kudsk, S., Miyake, F., Olsen, J.,  
934 Reinig, F., Sakamoto, M., Sookdeo, A., and Talamo, S.: The IntCal20 Northern Hemisphere  
935 Radiocarbon Age Calibration Curve (0–55 cal kBP), *Radiocarbon*, 62, 725–757,  
936 <https://doi.org/10.1017/RDC.2020.41>, 2020.
- 937 Richter, A., Rysgaard, S., Dietrich, R., Mortensen, J., and Petersen, D.: Coastal tides in  
938 West Greenland derived from tide gauge records, *Ocean Dyn.*, 61, 39–49,  
939 <https://doi.org/10.1007/s10236-010-0341-z>, 2011.
- 940 Saenko, O. A., Yang, D., and Myers, P. G.: Response of the North Atlantic dynamic sea  
941 level and circulation to Greenland meltwater and climate change in an eddy-permitting ocean  
942 model, *Clim. Dyn.*, 49, 2895–2910, <https://doi.org/10.1007/s00382-016-3495-7>, 2017.
- 943 Shotyk, W., Goodsite, M. E., Roos-Barraclough, F., Frei, R., Heinemeier, J., Asmund, G.,  
944 Lohse, C., and Hansen, T. S.: Anthropogenic contributions to atmospheric Hg, Pb and As  
945 accumulation recorded by peat cores from southern Greenland and Denmark dated using  
946 the  $^{14}\text{C}$  “bomb pulse curve,” *Geochim. Cosmochim. Acta*, 67, 3991–4011,  
947 [https://doi.org/10.1016/S0016-7037\(03\)00409-5](https://doi.org/10.1016/S0016-7037(03)00409-5), 2003.
- 948 Spada, G. and Melini, D.: SELEN4; (SELEN version 4.0): a Fortran program for solving the  
949 gravitationally and topographically self-consistent sea-level equation in glacial isostatic  
950 adjustment modeling, *Geosci. Model Dev.*, 12, 5055–5075, <https://doi.org/10.5194/gmd-12-5055-2019>, 2019.
- 952 The IMBIE Team: Mass balance of the Greenland Ice Sheet from 1992 to 2018, *Nature*, 579,  
953 233–239, <https://doi.org/10.1038/s41586-019-1855-2>, 2020.
- 954 Vogt, T.: Late-Quaternary Oscillations of Level in Southeast Greenland., Oslo: Dybwad  
955 1933., 44 pp., 1933.
- 956 Wada, Y., Lo, M.-H., Yeh, P. J.-F., Reager, J. T., Famiglietti, J. S., Wu, R.-J., and Tseng, Y.-  
957 H.: Fate of water pumped from underground and contributions to sea-level rise, *Nat. Clim.*  
958 *Change*, 6, 777–780, <https://doi.org/10.1038/nclimate3001>, 2016.
- 959 Wangner, D. J., Sicre, M., Kjeldsen, K. K., Jaeger, J. M., Bjørk, A. A., Vermassen, F., Sha,  
960 L., Kjær, K. H., Klein, V., and Andresen, C. S.: Sea Surface Temperature Variability on the  
961 SE-Greenland Shelf (1796–2013 CE) and Its Influence on Thrym Glacier in Nørre  
962 Skjoldungesund, *Paleoceanogr. Paleoclimatology*, 35,  
963 <https://doi.org/10.1029/2019PA003692>, 2020.
- 964 Wood, K. R. and Overland, J. E.: Early 20th century Arctic warming in retrospect, *Int. J.*  
965 *Climatol.*, 30, 1269–1279, <https://doi.org/10.1002/joc.1973>, 2010.

966 Woodroffe, S. A. and Long, A. J.: Salt marshes as archives of recent relative sea-level  
 967 change in West Greenland, *Quat. Sci. Rev.*, 28, 1750–1761, 2009.

968 Woodroffe, S. A. and Long, A. J.: Reconstructing recent relative sea-level changes in West  
 969 Greenland: local diatom-based transfer functions are superior to regional models, *Quat. Int.*,  
 970 221, 91–103, 2010.

971 Zheng, J.: Archives of total mercury reconstructed with ice and snow from Greenland and  
 972 the Canadian High Arctic, *Sci. Total Environ.*, 509–510, 133–144,  
 973 <https://doi.org/10.1016/j.scitotenv.2014.05.078>, 2015.

974

975

976